



HAL
open science

Virtual epileptic patient brain modeling: Relationships with seizure onset and surgical outcome

Julia Makhalova, Samuel Medina Villalon, Huifang Wang, Bernard Giusiano, Marmaduke Woodman, Christian Bénar, Maxime Guye, Viktor Jirsa, Fabrice Bartolomei

► **To cite this version:**

Julia Makhalova, Samuel Medina Villalon, Huifang Wang, Bernard Giusiano, Marmaduke Woodman, et al.. Virtual epileptic patient brain modeling: Relationships with seizure onset and surgical outcome. *Epilepsia*, 2022, 10.1111/epi.17310 . hal-03702938

HAL Id: hal-03702938

<https://hal.science/hal-03702938>

Submitted on 20 Sep 2023

HAL is a multi-disciplinary open access archive for the deposit and dissemination of scientific research documents, whether they are published or not. The documents may come from teaching and research institutions in France or abroad, or from public or private research centers.



L'archive ouverte pluridisciplinaire **HAL**, est destinée au dépôt et à la diffusion de documents scientifiques de niveau recherche, publiés ou non, émanant des établissements d'enseignement et de recherche français ou étrangers, des laboratoires publics ou privés.



Distributed under a Creative Commons Attribution - NonCommercial - NoDerivatives 4.0 International License

RESEARCH ARTICLE

Virtual epileptic patient brain modeling: Relationships with seizure onset and surgical outcome

Julia Makhalova^{1,2,3}  | Samuel Medina Villalon^{1,4} | Huifang Wang⁴ | Bernard Giusiano^{4,5} | Marmaduke Woodman⁴ | Christian Bénar⁴ | Maxime Guye^{1,2,3} | Viktor Jirsa⁴ | Fabrice Bartolomei^{1,4} 

¹APHM, Timone Hospital, Epileptology and Cerebral Rhythmology, Marseille, France

²CNRS, CRMBM, Aix Marseille University, Marseille, France

³APHM, Timone Hospital, CEMEREM, Marseille, France

⁴Aix Marseille Univ, INSERM, INS, Inst Neurosci Syst, Marseille, France

⁵APHM, Public Health Department, Marseille, France

Correspondence

Fabrice Bartolomei, Service d'Epileptologie et de Rythmologie Cérébrale, Hôpital Timone, 264 Rue Saint-Pierre, Marseille 13005, France. Email: fabrice.bartolomei@ap-hm.fr

Funding information

Agence Nationale de la Recherche, Grant/Award Number: ANR-17-RHUS-0004; Horizon 2020 Framework Programme, Grant/Award Number: 945539

Abstract

Objective: The virtual epileptic patient (VEP) is a large-scale brain modeling method based on virtual brain technology, using stereoelectroencephalography (SEEG), anatomical data (magnetic resonance imaging [MRI] and connectivity), and a computational neuronal model to provide computer simulations of a patient's seizures. VEP has potential interest in the presurgical evaluation of drug-resistant epilepsy by identifying regions most likely to generate seizures. We aimed to assess the performance of the VEP approach in estimating the epileptogenic zone and in predicting surgical outcome.

Methods: VEP modeling was retrospectively applied in a cohort of 53 patients with pharmaco-resistant epilepsy and available SEEG, T1-weighted MRI, and diffusion-weighted MRI. Precision recall was used to compare the regions identified as epileptogenic by VEP (EZ_{VEP}) to the epileptogenic zone defined by clinical analysis incorporating the Epileptogenicity Index (EI) method (EZ_C). In 28 operated patients, we compared the VEP results and clinical analysis with surgical outcome.

Results: VEP showed a precision of 64% and a recall of 44% for EZ_{VEP} detection compared to EZ_C . There was a better concordance of VEP predictions with clinical results, with higher precision (77%) in seizure-free compared to non-seizure-free patients. Although the completeness of resection was significantly correlated with surgical outcome for both EZ_C and EZ_{VEP} , there was a significantly higher number of regions defined as epileptogenic exclusively by VEP that remained nonresected in non-seizure-free patients.

Significance: VEP is the first computational model that estimates the extent and organization of the epileptogenic zone network. It is characterized by good precision in detecting epileptogenic regions as defined by a combination of visual analysis and EI. The potential impact of VEP on improving surgical prognosis remains to be exploited. Analysis of factors limiting the performance of the actual model is crucial for its further development.

This is an open access article under the terms of the [Creative Commons Attribution-NonCommercial-NoDerivs](https://creativecommons.org/licenses/by-nc-nd/4.0/) License, which permits use and distribution in any medium, provided the original work is properly cited, the use is non-commercial and no modifications or adaptations are made.

© 2022 The Authors. *Epilepsia* published by Wiley Periodicals LLC on behalf of International League Against Epilepsy.

KEYWORDS

epilepsy, personalized brain modeling, SEEG, seizure onset zone, surgical prognosis

1 | INTRODUCTION

Epilepsy surgery represents the only potentially effective treatment to achieve seizure control in patients suffering from drug-resistant focal epilepsy. Recent US¹ and European² surveys have shown interesting trends over the past 2 decades, with an increase in the number of complex cases and an increase in the use of invasive explorations, contrasting with a very modest improvement in prognosis. Stereoelectroencephalography (SEEG) has become the reference invasive method at a growing number of centers worldwide.^{3–6} However, despite apparent technical advances, the success rate of surgery remains less favorable in cases requiring intracerebral electroencephalographic (EEG) exploration, and does not overcome a 60% ceiling as demonstrated by the SEEG-based surgical series.^{5,7,8} Therefore, improving the indications, management, and prognosis of epilepsy surgery remains the major challenge of ongoing research. Defining the epileptogenic zone (EZ) based on SEEG interpretation can be difficult,⁹ because the patterns of seizure onset and early spread may present a complex organization, underpinned by a network organization.^{8,10,11} The term “epileptogenic network” has been proposed to better reflect this complexity.¹² Signal quantification methods that measure either spectral content of SEEG signals or changes in functional connectivity have emerged over the past decade, to better analyze the EZ and facilitate the interpretation of SEEG data. In particular, indices based on the detection of fast activities have been proposed, with a visualization of the results in magnetic resonance imaging (MRI).^{13–16} The most used method is the Epileptogenicity Index (EI),¹³ which allows detection of changes in the proportion of fast activity detached from the background activity, taking into account the succession of timing of involvement of a given region in the seizure. The implementation of quantitative approaches has accompanied a major conceptual and theoretical evolution in epilepsy surgery, from the concept of epileptogenic focus and several definitions of different zones (e.g. the EZ, the seizure onset zone, and the irritative zone)^{17–20} toward the concept of epileptogenic networks.^{12,21,22} Accordingly, the EZ network (EZN) is conceptualized as a network of connected hyperexcitable regions capable of generating seizures.¹²

More recently, methods of for computational large-scale modeling of the epileptic brain have been introduced.^{23–26} The principle of computational neuronal models is to reproduce and explain different types of

Key Points

- VEP is the first computational model that offers 3D imaging of the epileptogenic zone network.
- The VEP model shows good precision in detecting epileptogenic regions as compared to current state-of-the-art model-free approaches.
- VEP can provide information on brain regions not sampled by SEEG electrodes.
- The completeness of resection of the epileptogenic zone predicted by VEP correlated with surgical outcome.

epileptiform activity.²⁷ By integrating a dynamic computational neuronal model, capable of simulating seizure-like activity (i.e., a phenomenological neural mass model [NMM]) into the large-scale brain network, model-based approaches allow modeling of seizures inside a patient's brain.

The virtual epileptic patient (VEP) is a novel, multimodal probabilistic modeling framework, based on Virtual Brain²⁸ technology. VEP uses personalized brain network models and machine learning methods by integrating epilepsy patient-specific anatomical with functional data to provide a computational representation of the hypothesized epileptogenic and propagation zone networks in cerebral space. This method has recently been validated by modeling seizures previously recorded in SEEG^{24,29} and on synthetic data.^{30,31} The pilot study by Proix et al.²⁹ further showed that VEP can reliably predict seizure propagation, suggesting that in the future this approach could improve SEEG analysis and consequently surgical prognosis.

In this work, we aimed to demonstrate the feasibility of VEP modeling in identifying the EZN of patients who underwent SEEG and surgery. We assessed the predictive power of VEP in detecting epileptogenic regions, as compared to the clinical analysis combined with the EI method, and to the surgical outcome.

2 | MATERIALS AND METHODS

2.1 | Patients and data acquisition

VEP modeling was retrospectively applied in a cohort of 53 patients suffering from drug-resistant focal epilepsy,

with available SEEG seizure recordings, and three-dimensional (3D) T1-weighted and diffusion-weighted MRI. All patients underwent comprehensive presurgical assessment including medical history, neurological examination, neuropsychological assessment, fluorodeoxyglucose positron emission tomography, high-resolution 3-T MRI, long-term scalp video-EEG, and subsequent SEEG monitoring. Follow-up information was collected from a review of the medical records. Surgical outcome, if applicable, was assessed according to Engel classification. Informed written consent was obtained for all patients, and the study was approved by the local ethics committee (Comité de Protection des Personnes sud Méditerranée 1).

2.2 | MRI acquisitions

All images were acquired on a Siemens Magnetom Verio 3-T magnetic resonance scanner. MRI acquisitions included a 3D T1-weighted magnetization-prepared rapid gradient echo (3D-MPRAGE) sequence (repetition time = 1.9 or 2.3 s, echo time = 2.19 or 2.98 ms, spatial resolution = $1.0 \times 1.0 \times 1.0 \text{ mm}^3$) and a diffusion-weighted MRI (DW-MRI) sequence (either with an angular gradient set of 64 directions, repetition time = 10.7 s, echo time = 95 ms, voxel size = $1.95 \times 1.95 \times 2.0 \text{ mm}^3$, b-weighting of 1000 s/mm^2 or with an angular gradient set of 200 directions, repetition time = 3 s, echo time = 88 ms, voxel size = $2.0 \times 2.0 \times 2.0 \text{ mm}$, b-weighting of 1800 s/mm^2). Patients also underwent conventional 3-T MRI according to the standardized presurgical epilepsy assessment protocol. Postoperative MRI was performed 3 months after surgery.

2.3 | SEEG recording

The SEEG recordings were performed as a part of routine clinical management, in line with the French national guidelines,⁶ to determine the EZ and its relations with eloquent areas. SEEG implantation was planned individually for each patient, according to the hypotheses about the localization of the EZ based on noninvasive investigations. All SEEG explorations were bilateral, predominantly on the side of the hypothesized main EZ, with some contralateral electrodes, and systematically sampled temporal, insular, frontal, and parietal regions of at least one hemisphere. Intracerebral multiple contact electrodes (10–18 contacts with length = 2 mm, diameter = .8 mm, 1.5 mm apart, Alcis) were placed stereotactically by using the robotized surgical assistant ROSA. A postimplantation computed tomography (CT) scan was performed to

check the implantation accuracy and exclude intracranial bleeding. Signals were recorded on a Natus system with sampling at 512 Hz or 1024 Hz and 16-bit resolution, using a hardware high-pass filter (cutoff at .16 Hz at -3 dB) and a hardware antialiasing low-pass filter (cutoff at 170 Hz or 340 Hz, respectively).

2.4 | SEEG signal analysis

All signal analyses were performed in a bipolar montage using the open source AnyWave software³² available at <https://meg.univ-amu.fr/wiki/AnyWave>. The epileptogenic regions were defined by two expert clinicians (F.B. and J.M.), based on visual and quantitative SEEG signal analysis using the EI method.¹³ A normalized EI value, ranging from 0 (no epileptogenicity) to 1 (maximal epileptogenicity) was used for each considered structure (for detailed methodology see Bartolomei et al.¹³). In each patient, maximal EI values from at least three representative seizures (when available) were computed for all bipolar SEEG contacts. The same SEEG datasets of each respective patient were used for the data fitting within the VEP pipeline.

2.5 | VEP workflow

The VEP workflow³¹ methodological details are provided in Appendix S1 and Figure S1. In brief, the virtual brain model defines the brain as a network of 162 regions, each representing a node in the network. These regions are delineated by the VEP atlas, a cortical and subcortical parcellation of the brain developed specifically for use in epileptology and functional neurosurgery (available at <https://ins-amu.fr/vep-atlas>).³³ Brain regions are automatically labeled, based on the patients' 3D-MPRAGE images (further referred to as T1-MRI). Connections between regions are estimated through streamline tractography from DW-MRI. The MRtrix3 software package was used to process the DW-MRI, by employing constrained spherical deconvolution to derive the fiber orientation distribution functions and a probabilistic algorithm to sample 15 million tracts.³⁴ The structural connectome was constructed by assigning and counting the streamlines to and from each VEP brain region. In this way, a patient-specific structural connectivity matrix is obtained, which defines the links and the connection strength between the nodes of the network. The dynamics of each node are defined by an NMM, which is a system of nonlinear differential equations, the Epileptor,³⁵ that represents the neural activity in that brain region. The source signals generated by the Epileptor at the

brain region level are mapped upon the sensor signals measured by the SEEG electrodes. The electromagnetic forward problem is solved by the gain matrix, which is a function of the distance between the sources and sensors.³⁶ It is obtained by localizing the SEEG electrodes in patient-specific MRI space using the open source software GARDEL (Graphical user interface for Automatic Registration and Depth Electrodes Localization),³⁷ available at <https://meg.univ-amu.fr/wiki/GARDEL:preregistration>. Coregistration of the T1-MRI with postimplantation CT images was performed, followed by an automatic recognition and anatomical localization of each electrode contact, which was then assigned automatically to the respective anatomical region of the VEP atlas projected in the patient's MRI space. Thus, the source space covers the whole brain, that is, the 162 brain regions defined by the VEP atlas, whereas the sensors sample only some of those regions, depending on the SEEG implantation scheme.

A Bayesian modeling approach is applied to infer the epileptogenicity parameters and source time series for each seizure. The VEP workflow automatically runs through the clinical data, including structural connectivity from DW-MRI, patient-specific brain space from T1-MRI, and functional SEEG data, without predetermining the ictal zone. Machine learning and artificial intelligence are used to estimate the patient-specific parameters of the model. The model inversion module allows inferring each region's epileptogenicity by fitting the SEEG data features. The inputs of the model inversion module are the data feature and a prior. The envelope of signal power (high-pass filtered signal followed by envelope smoothing) from empirical SEEG recordings serves as the data feature. The data features are extracted during the periods of interictal to ictal transition and may extend until the seizure end, whereas the interictal activity is regarded as a baseline. The prior is computed using signal processing of raw SEEG data based on the channels' spectral content across 52 different frequency bands (10–110 Hz), weighted by the seizure onset delay in each channel. It maps a weighted sum of the prior epileptogenicity values of all sensors to each source, based on their distance. The output of the model inversion module is a distribution of epileptogenicity values (EV), which are determined by the key parameters from the model inversion and the patient's structural connectivity. An overview of the most relevant brain regions is presented in the VEP report table, including the information on highlighted brain regions with the distribution of the estimated EV and the EZ definition (yes/no) based on EV. The regions are defined as epileptogenic with a threshold of $EV > .5$. They are displayed in red in the three classical planes of the patient's 3D T1-MRI, called a heatmap.

2.6 | Definition of regions of interest

Brain regions defined according to the VEP atlas parcellation³³ were used as regions of interest. Two clinical experts (F.B., J.M.) labeled each brain region as belonging to the EZN, the propagation zone network (PZN), or the noninvolved zone (NIZ), based on the clinical analysis incorporating the EI.³⁸ An $EI \geq .4$ was set as a threshold to define a region as the EZN. Brain regions with $.1 < EI < .4$ and sustained discharge during the seizure were defined as the PZN; all other regions were defined as the NIZ. If a region was sampled by two or more bipolar contacts, the maximal EI value obtained for this region was used. The EZN regions were defined as clinical hypothesis (EZ_C) for further analysis. The regions predicted as epileptogenic by VEP were defined as EZ_{VEP} for further analysis.

2.7 | Resection extent estimation

For the operated patients, the extent of resection of different brain regions was defined using GARDEL software. The coregistration of the postimplantation CT with electrodes with the postoperative MRI, and that of the post- and preoperative MRI were performed. The resected contacts were identified by visual inspection and assigned to the respective VEP atlas regions as defined by the preoperative MRI (see above). The regions resected but not explored by depth electrodes were then identified visually on the pre-/postoperative MRI coregistered images (S.M.V., J.M.). The completeness of resection of each region was estimated visually by two trained clinicians (F.B., J.M.). A VEP region was defined as resected if at least 50% of it was resected, with respect to its major axis length. Otherwise, it was considered as nonresected. For both, EZ_C and EZ_{VEP} regions, a “resected” or “nonresected” status was then assigned.

2.8 | Statistical analysis

Statistical analyses were performed using MATLAB statistics toolbox (15.0 and 18.0). Precision recall was used as a performance measure to compare the epileptogenic regions predicted by VEP (EZ_{VEP}) against the clinical analysis incorporating the EI method (EZ_C), considered as standard. We assessed VEP model performances (1) in the whole cohort of 53 patients, (2) according to surgical outcome (seizure-free vs. not seizure-free patients), and (3) according to brain region topography: mesial versus lateral, temporal versus extratemporal. The latter was assessed for 28 regions, each sampled in at least 10 patients.

Two-sided Wilcoxon test was used to assess group differences in the extent of resection of EZ_C and EZ_{VEP}, the number of nonresected epileptogenic regions, the number of EZ_{VEP} regions not identified as epileptogenic by the clinical approach, and the number of EZ_{VEP} regions not sampled by SEEG, between the seizure-free and non-seizure-free patients. A *p*-value < .05 was considered as significant.

2.9 | Data availability

The complete VEP workflow is available in Appendix S1. VEP atlas parcellation is available open source at <https://ins-amu.fr/vep-atlas>. The other data that support the findings of this study are available from the corresponding author upon reasonable request.

3 | RESULTS

3.1 | Clinical features

Patients' clinical data are summarized in Table 1 (for detailed characteristics, see Table S1). Fifty-three patients (25 males, 28 females) were included. Mean age at epilepsy onset was 16.2 years (range = .1–55), mean duration of epilepsy was 17.2 years (range = 3–45), and mean age at evaluation was 33.4 years (range = 15–60). An MRI-visible structural abnormality was present in 64% of cases, whereas 36% had unremarkable MRI findings. The EZ organization according to the clinical hypothesis incorporating EI was unilateral in 39, bilateral in 11, and unilateral multifocal in two cases. The EZ was topographically limited to the temporal lobe in 20 cases (37.7%), whereas it was extratemporal or temporal Plus³⁹ in 33 patients (62.3%). Within the temporal Plus subgroup, two thirds were temporofrontal and temporoinsular epilepsies, followed by temporoparietal, temporo-occipital, and more complex, temporooperisylvian EZ organization. Among the extratemporal cases, the posterior epilepsies were most frequent, followed by frontal, motor–premotor, insular–opercular, and frontoinsular epilepsies (Figure 1A). 28 of 53 patients underwent curative surgical procedures. The postsurgical outcome was favorable in 18 (Engel Class I, 50%; Engel Class II, 14%), with worthwhile improvement in six (Engel Class III, 22%), and without significant improvement in four cases (Engel Class IV, 14%).

3.2 | VEP model performance as compared to clinical and EI estimation

VEP model detected a total of 198 epileptogenic regions in 53 patients (mean number per patient = 3.74 ± 2.2 ,

TABLE 1 Patient clinical data

Age, years	33.4 ± 10.51 (15–60)
Sex, male/female	25/28
Age at epilepsy onset, years	16.2 ± 12.95 (.1–55)
Epilepsy duration, years	17.2 ± 9.56 (3–45)
Side, left/right/bilateral	21/21/11
MRI, normal/lesion, % (<i>n</i>)	36% (19)/64% (34)
Surgery, % (<i>n</i>)	52.8% (28)
Tailored resection, <i>n</i>	18
ATL, <i>n</i>	8
Disconnection, <i>n</i>	1
Gamma knife, <i>n</i>	1
Outcome, Engel class, % (<i>n</i>)	
I	50% (14)
II	14% (4)
III	22% (6)
IV	14% (4)
Histopathology, <i>n</i>	
FCD	9
Hippocampal sclerosis	6
Ganglioglioma	1
Gliosis	9
Nonoperated, % (<i>n</i>)	47.2% (25)
Bilateral or multifocal EZ, <i>n</i>	13
High risk of functional deficit, <i>n</i>	7
Seizure-free after SEEG, <i>n</i>	1
Seizure-free after TC, <i>n</i>	3
Patient refused surgery, <i>n</i>	1

Note: Data are presented as mean ± SD (range) or % (*n*).

Abbreviations: ATL, anterior temporal lobectomy; EZ, epileptogenic zone; FCD, focal cortical dysplasia; MRI, magnetic resonance imaging; SEEG, stereoelectroencephalography; TC, thermocoagulations.

range = 1–10). Eighty-four detections (42%) in 40 patients were not identified as epileptogenic by visual SEEG analysis or the EI. Among these additionally detected regions, 25 (29.8%) were not sampled by SEEG electrodes, 28 (33.3%) were within the clinically defined propagation network, and the remaining 31 (36.9%) were considered to be noninvolved based on visual analysis and the EI. The total number of additional VEP detections was significantly higher in non-seizure-free patients compared to the seizure-free subgroup (*p* = .05, Wilcoxon). In the same way, the number of detected regions without SEEG sampling was significantly higher in the non-seizure-free group (*p* = .04, Wilcoxon).

We compared the regions identified as EZ_{VEP} against the EZ_C by using precision recall. The results of the whole cohort of 53 patients show a mean precision of .64 and

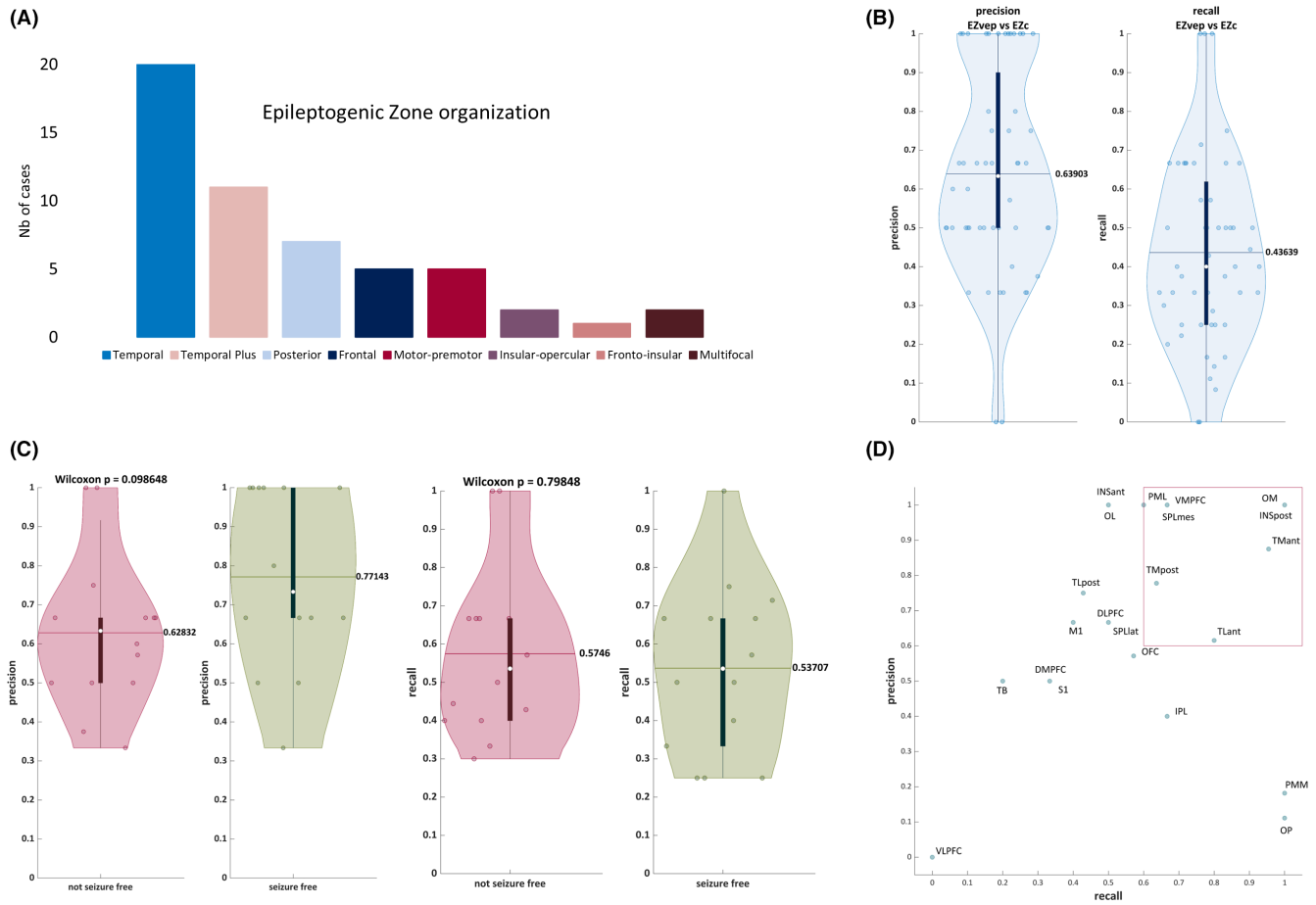


FIGURE 1 Virtual epileptic patient (VEP) model performance compared to clinical gold standard. (A) Epileptogenic zone (EZ) organization according to the clinical analysis incorporating the Epileptogenicity Index (EI) method.¹³ (B) Precision/recall EZ_{VEP} (EZ predicted by VEP) versus EZ_C (EZ defined by clinical analysis incorporating the EI) in a whole cohort of 53 patients. (C) The same statistical analysis in a cohort of 28 operated patients, comparing the seizure-free and the non-seizure-free groups. There is a clear trend toward better precision in the seizure-free group ($p = .09$, Wilcoxon). (D) Precision/recall per brain region. DLPFC, dorsolateral prefrontal cortex; DMPFC, dorsomedial prefrontal cortex; INSant, anterior insula; INSpost, posterior insula; IPL, inferior parietal lobule; M1, primary motor cortex; OFC, orbitofrontal cortex; OL, occipital lateral; OM, occipital mesial; OP, parietal operculum; PML, lateral premotor cortex; PMM, mesial premotor cortex; S1, primary sensory cortex; SPLlat, lateral superior parietal lobule; SPLmes, mesial superior parietal lobule; TB, temporal basal; TLant, anterior temporal lateral; TLpost, posterior temporal lateral; TMant, anterior temporal mesial; TMpost, posterior temporal mesial; VLPFC, ventrolateral prefrontal cortex; VMPFC, ventromesial prefrontal cortex.

a mean recall of .44 (Figure 1B). The recall is better in MRI-negative cases (.54) compared to lesional cases (.38, $p < .05$), both subgroups showing precision of .68 and .62, respectively. Regarding the epilepsy types according to the EZ organization, the recall is significantly better in the temporal subgroup (.50) compared to the temporal Plus subgroup (.32, $p < .05$), and it does not differ significantly in the extratemporal subgroup (.44) compared to each of these subgroups. The precision remains comparable (.65, .60, and .63, respectively) between these subgroups. When focusing on the 28 operated patients (Figure 1C), the recall is .57 in seizure-free and .54 in non-seizure-free patients, and there is a clear trend to a better precision in the seizure-free (.77) compared to non-seizure-free group (.63), however, without reaching statistical significance

($p = .09$, Wilcoxon). VEP performs better in detecting temporal than extratemporal (precision .62 vs .53; recall .42 vs .33) as well as mesial than lateral regions (precision .70 vs .46; recall .44 vs .32; Figure 1D).

3.3 | Correlation between the extent of EZ resection and surgical outcome

We assessed correlation between the extent of the EZ resection and surgical outcome (Figure 2). The percentage of resected epileptogenic regions was significantly higher in the seizure-free group compared to non-seizure-free patients, considering EZ_C ($.92 \pm .17$ vs. $.67 \pm .28$, $p < .01$) or EZ_{VEP} ($.91 \pm .19$ vs. $.55 \pm .26$, $p < .01$; Figure 2A). In line

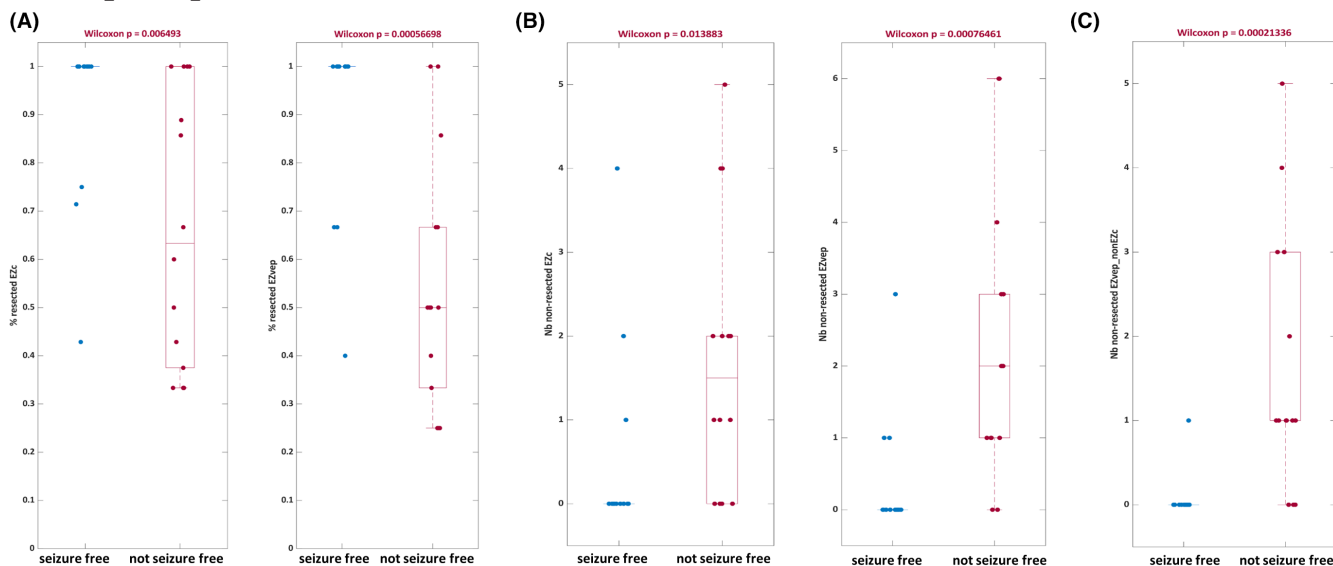


FIGURE 2 Correlation between the extent of the epileptogenic zone (EZ) resection and surgical outcome. (A) The percentage of resected epileptogenic regions was significantly higher in seizure-free compared to non-seizure-free patients, both when the EZ was defined by clinical analysis incorporating the Epileptogenicity Index (EZ_C) and when predicted by the virtual epileptic patient (EZ_{VEP}). (B) The number of nonresected epileptogenic regions was significantly higher in the non-seizure-free group, for both EZ_C (left) and EZ_{VEP} (right). (C) The number of nonresected epileptogenic regions identified by the VEP but not by clinicians ($EZ_{VEP_non-EZ_C}$) was also significantly higher in the non-seizure-free group.

with this finding, the number of nonresected EZ regions was significantly higher in the non-seizure-free group than in the seizure-free group, for both EZ_C (1.71 ± 1.63 vs. $.5 \pm 1.16$, $p = .01$) and EZ_{VEP} (2.36 ± 1.95 vs. $.36 \pm .84$, $p < .01$; Figure 2B). Importantly, the number of nonresected epileptogenic regions that were predicted by the model but not detected as such by clinicians was also significantly higher in the non-seizure-free versus seizure-free group (1.64 ± 1.55 vs. $.07 \pm .27$, $p < .01$; Figure 2C).

3.4 | VEP model performance at individual patient level: Illustrative situations

Different clinical situations are illustrated in Figures 3–5. Figure 3 shows a case with a good concordance between the clinical hypothesis and the model prediction. Figure 4 shows a case where a region interpreted as epileptogenic by clinicians (and detected by EI) was not predicted by the VEP model. Figure 5 shows a case demonstrating excellent precision of the VEP compared to clinical hypothesis and its added diagnostic value in detecting an epileptogenic region.

A detailed analysis of 11 seizure-free patients, for whom seizure freedom was achieved by resections including 100% of the EZ predicted by VEP, was performed. The EZ_{VEP} and EZ_C matched completely in one case and were partially overlapping in five cases; the EZ_{VEP} was more

extended than the EZ_C in one case, whereas four patients had the EZ_{VEP} less extended than the resected EZ_C . Of the latter, three cases were temporofrontal EZN, with VEP failing to detect the prefrontal regions, and one case was parietal EZN, with VEP failing to detect the postcentral regions. All these missed regions contained an MRI-visible lesion.

4 | DISCUSSION

The development of SEEG over the past 15 years has seen the need to quantify the recorded electrophysiological activities, particularly during seizure genesis.^{40,41} In this perspective, there are several possible solutions that can be separated into model-free approaches based on the processing of the signal itself and model-based approaches using computational modeling. The former use SEEG signal quantification,^{13,14,16,42} or network-based analysis of SEEG or magnetoencephalography (MEG) recordings,^{43,44} whereas the latter implement computational large-scale brain modeling fitted by SEEG data from ictal^{23–25,45} or interictal²⁶ recordings, both employing machine learning and artificial intelligence. All of them aim to facilitate the SEEG interpretation and surgical decision-making. However, most of the previous research in the field has focused either on the prediction of surgical outcome, or on testing the virtual resection scenarios^{23,45,46–48} or the prediction of seizure propagation.^{29,31} The present study

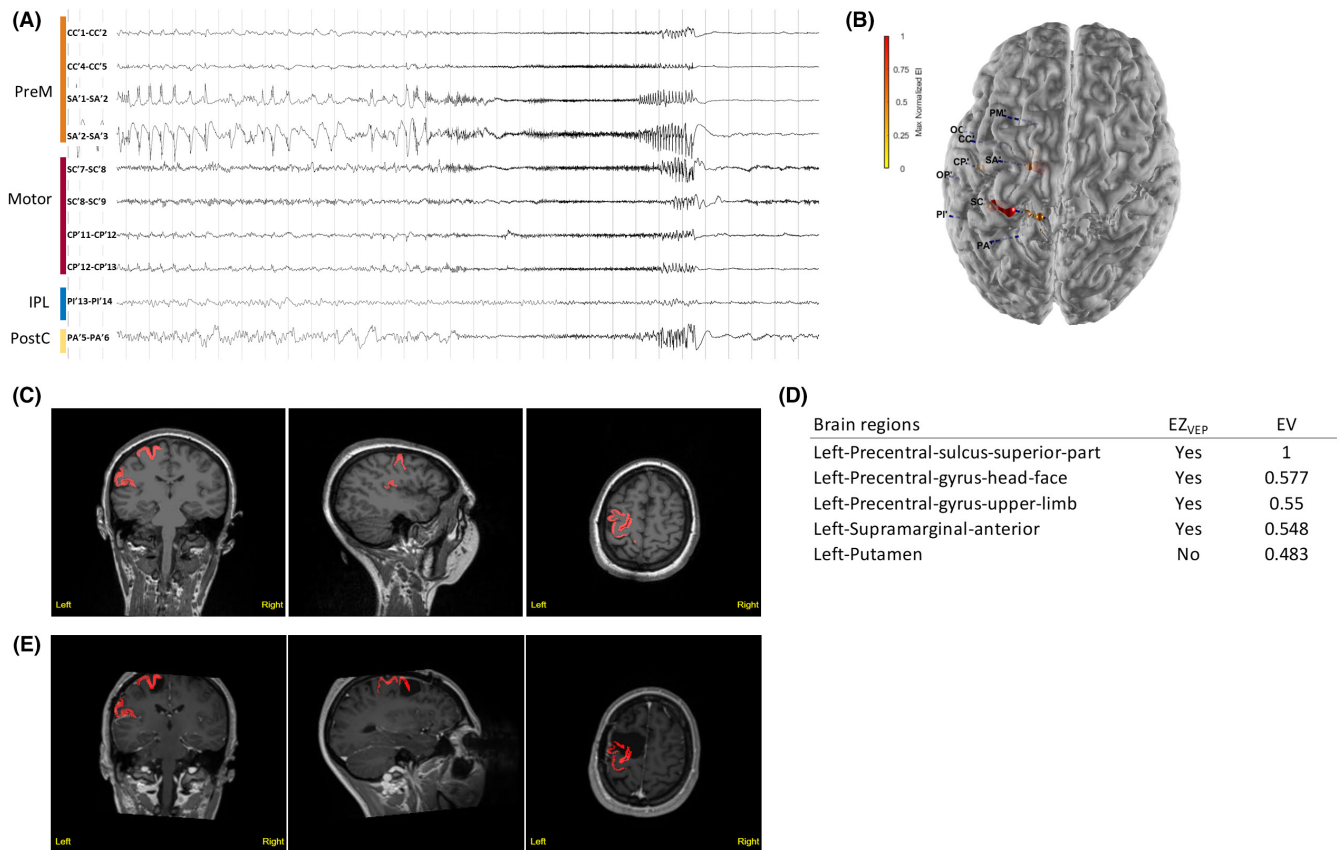


FIGURE 3 Illustrative Case 1. Motor–premotor epileptogenic zone (EZ) network is shown. The subject was a 23-year-old woman with sleep-related, focal aware tonic seizures (tonic posture of the right arm) and negative magnetic resonance imaging (MRI). (A) Stereoelectroencephalographic (SEEG) recordings of a habitual seizure that starts from the left premotor and primary motor regions. IPL, inferior parietal lobule; PostC, the postcentral cortex; PreM, premotor cortex. (B) Patient’s three-dimensional (3D) brain mesh with SEEG electrodes. The maximal Epileptogenicity Index (EI) values are represented as spheres on the respective contacts according to a color map. The EI shows maximal epileptogenicity within the left supplementary motor area, the precentral gyrus and central sulcus, the precentral sulcus in its superior part, and the left caudal superior frontal sulcus. (C, D) Clinical report: heatmap (C) and list of brain regions with respective epileptogenicity values (EV; D). Regions identified as EZ_{VEP} (EZ predicted by the virtual epileptic patient) are displayed in red on the coronal, sagittal, and axial views of the patient’s 3D T1-MRI, also available as 3DViewer in HTML format. The color intensity varies according to the median of epileptogenicity. (E) Heatmap showing EZ_{VEP} regions on the postoperative T1-MRI. The EZ_{VEP} included premotor–motor regions (left precentral sulcus, superior part; left precentral gyrus, head–face; and left precentral gyrus, upper limb) and left supramarginal gyrus, anterior. The patient benefited from a tailored resection of the left lateral and mesial premotor cortex, sparing the central region. The extent of resection of EZ_C (EZ defined by clinical analysis incorporating the EI) was estimated as 43% and that of EZ_{VEP} as 25%. The patient had residual focal aware seizures with clonic jerks of the right hand, a semiology suggestive of seizure origin in the primary motor cortex.

demonstrates that it is possible to define the EZN from SEEG data by using VEP large-scale brain modeling. Herein, the VEP approach has been applied in a cohort of 53 patients with drug-resistant focal epilepsy explored by SEEG, well representative of patient populations reported in recent surgical series.^{5,7}

The VEP implements the concept of epileptogenic networks^{12,22} and brings together functional imaging from SEEG recordings and large-scale brain modeling at an individual patient level. VEP estimates the epileptogenicity of brain regions represented as nodes of the brain network with a structural resolution of 81 regions per hemisphere.

It provides results in terms of epileptogenic brain regions (at source level), which are complementary with the EZN quantification by the EI,¹³ or by other SEEG quantification methods.⁴¹ The latter are based on the detection of fast activities at seizure onset, eventually combined with other metrics, for example, with nonlinear regression coefficient h^2 in the newly proposed Connectivity Epileptogenicity Index,⁴² statistical estimate of the gamma power in epileptogenicity maps,^{14,49} slow polarizing shift and background flattening,¹⁵ or preictal spikes and suppression of low frequencies in the fingerprint.¹⁶ Importantly, all these methods estimate epileptogenicity at the level of recording

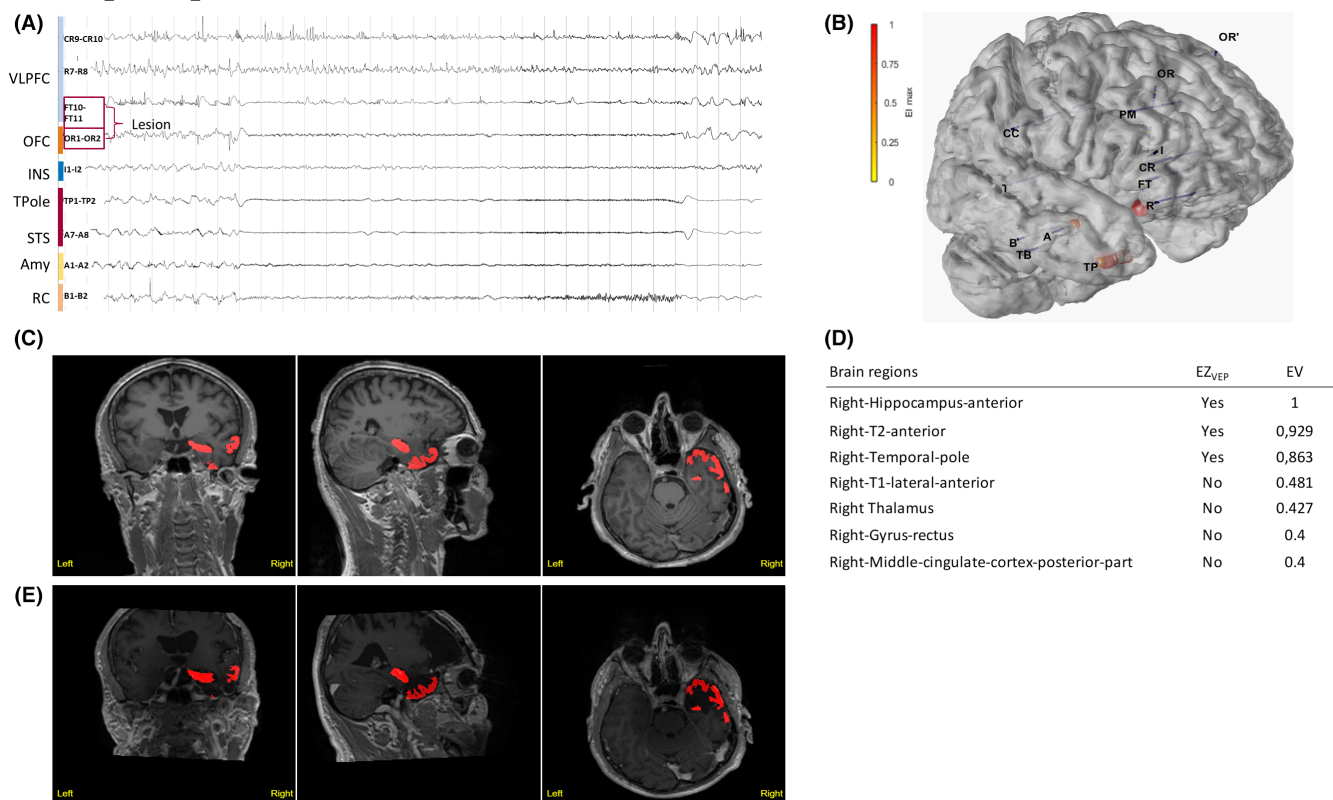


FIGURE 4 Illustrative Case 2. Temporofrontal epileptogenic zone (EZ) network is shown. A 56-year-old right-handed man suffered from focal drug-resistant epilepsy since the age of 11 years. He experienced weekly focal seizures with impaired awareness, with subjective signs including anxiety or fear, ascending epigastric sensation and chills, and as objective semiology, verbal and gestural automatisms, as well as hypermotor behavior during nocturnal seizures. His magnetic resonance imaging (MRI) was suggestive of a focal cortical dysplasia (FCD) within the right orbitofrontal cortex (OFC) and fronto-opercular region. (A) Stereoelectroencephalography (SEEG) recordings of a habitual seizure. The seizure starts with rapid discharge in gamma-band within the right anterior temporal structures and the OFC, whereas the opercular part of the lesion is not involved. Amy, amygdala; INS, insula; RC, rhinal cortex; STS, superior temporal sulcus; TPole, temporal pole; VLPFC, ventrolateral prefrontal cortex. (B) The patient's three-dimensional (3D) brain mesh with implanted SEEG electrodes showing the maximal Epileptogenicity Index (EI) values within the right OFC, the amygdala, the temporal pole, and the superior temporal sulcus. (C, D) Clinical report. (C) Heatmap displays regions identified as EZ_{VEP} (EZ predicted by the virtual epileptic patient) in red on the patient's 3D T1-MRI. (D) List of detected brain regions with respective epileptogenicity values (EV). (E) Heatmap showing EZ_{VEP} regions on the postoperative T1-MRI. EZ_{VEP} included the right anterior temporal lobe (the temporal pole, the anterior hippocampus, and the anterior T2), but not the right orbitofrontal region. A tailored resection including the lateral prefrontal and orbitofrontal lesional and perilesional cortex, as well as the right anterior temporal lobe, led to complete seizure freedom (Engel Class I at 9-year follow-up), without any functional deficit. The extent of resection was 100% for both EZ_C (EZ defined by clinical analysis incorporating the EI) and EZ_{VEP} . The histopathological finding was right frontal FCD type 2b. The interpretation in this situation is not univocal. Either this region was not epileptogenic and resection could have spared it, or the region was epileptogenic and here the VEP lacks sensitivity.

electrodes (sensor level) and are therefore limited by the sampling problem, which is resolved by the VEP approach operating, as mentioned above, on the whole brain scale.

In the present retrospective study, the concordance of VEP predictions with clinical analysis incorporating the EI was .64 for the precision and .44 for the recall. The recall was significantly higher in MRI-negative cases (.54) compared to lesional cases (.38, $p < .05$), as well as in temporal (.50) compared to temporal Plus (.32, $p < .05$) cases, whereas the precision remained equal among these subgroups. These results highlight good predictive value of the current VEP prototype in detecting

the regions defined as epileptogenic by clinician and SEEG signal analysis, as well as the robustness of the VEP approach, when applied in a "real life" patient cohort with heterogeneous profiles of EZ organization and temporal Plus³⁹ or extratemporal EZ accounting for more than half of cases. Moreover, in a subgroup of 28 operated patients, higher concordance between the EZ predicted by the model and clinical EZ hypothesis was associated with better surgical outcome (precision = .77 in the seizure-free group), although not reaching statistical significance due to a small sample size. These data are in good agreement with a study by Proix et al.²⁹ that

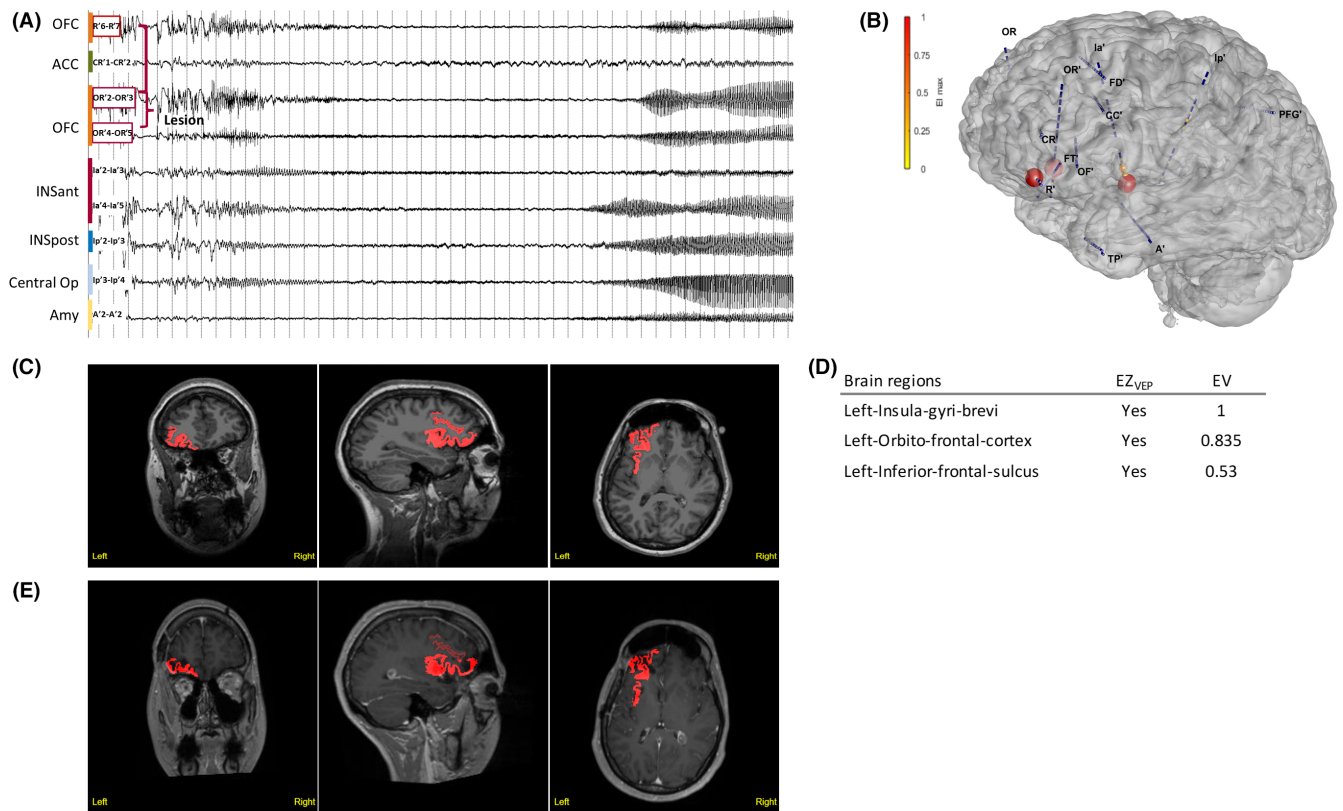


FIGURE 5 Illustrative Case 3. Prefrontoinsular epileptogenicity value (EV) network. A 29-year-old left-handed woman presented with sleep-related hyperkinetic focal seizures with impaired awareness that occurred in clusters several times per week. The patient's 7-T brain magnetic resonance imaging (MRI) showed possible focal cortical dysplasia (FCD) in the left orbitofrontal cortex. High-resolution electroencephalography (standardized low-resolution electromagnetic tomography) showed source localizations within the left inferior frontal sulcus, the left orbitofrontal cortex, and the left anterior cingulum. (A) Stereoelectroencephalography (SEEG) recordings of a habitual seizure starting with a burst of polyspikes followed by low-voltage fast activity discharge that simultaneously involves the left orbitofrontal cortex (OFC), the anterior (INSant), and the posterior insula (INSpost), as well as the central operculum (Central Op). ACC, anterior cingulate cortex; Amy, amygdala. (B) The patient's three-dimensional (3D) brain mesh with SEEG electrodes showing the maximal Epileptogenicity Index (EI) values within the left OFC and the anterior insula. (C, D) Clinical report: (C) Heatmap showing regions identified as EZ_{VEP} (epileptogenic zone predicted by the virtual epileptic patient) in red on the patient's 3D T1-MRI. (D) List of detected brain regions with EV indicated. (E) Heatmap showing EZ_{VEP} regions on the postoperative T1-MRI. The EZ_{VEP} included the same structures as EI, and additionally, the left inferior frontal sulcus. Surgical resection comprised the left orbitofrontal and the anterior insular cortex, corresponding to the clinically defined EZ. The extent of EZ_{VEP} resection was 67%. Nocturnal seizures relapsed 1 month after surgery, but with significant reduction in seizure frequency compared to baseline (Engel Class III at 1-year follow-up). Histopathology showed left orbitofrontal FCD type 2a and no abnormality within the insular cortex. Magnetoencephalography performed 1 year after surgery showed source localizations within the left frontal operculum and the small residual part of the left anterior insula. Additional cortectomy including the left inferior frontal sulcus, detected by VEP, as well as the left frontal operculum, and the residual anterior insula has been planned.

demonstrated the same trend for the modeling of the PZN. They further confirm a global trend that predictive accuracy of model-based or network-based approaches implementing machine learning is likely better in seizure-free than in non-seizure-free patients.⁵⁰ One of the most pertinent findings of our study is that the completeness of resection of the EZ predicted by VEP significantly correlated with surgical outcome (91% in seizure-free vs. 55% in non-seizure-free, $p < .01$), independently from its concordance with clinical hypothesis. However, in one third of seizure-free patients with completely removed EZ_{VEP}, resections were extended

beyond its limits and included the regions not detected by VEP but considered epileptogenic by clinical hypothesis. The interpretation of such discordant results in the frame of a retrospective study is not univocal. Either these regions were not epileptogenic and could have been spared, or they were epileptogenic and here the VEP lacks sensitivity. Nonetheless, when applied prospectively in complex situations, such as illustrated in the Use Case 2, VEP might be helpful in confirming the extent of the EZ beyond the MRI-visible lesion. These results suggest the importance of the ongoing prospective French multicenter trial EPINOV (NCT03643016),

whose main objective is to estimate the potential impact of VEP on improving surgical prognosis in patients undergoing SEEG.

We further demonstrated that some regions predicted as epileptogenic by VEP were not detected by either visual SEEG analysis or the EI. One third of these detections corresponded to the regions with no available SEEG sampling. This illustrates that the VEP model can help estimate brain epileptogenicity with parameters that are not directly measurable from empirical observation. Because the number of nonresected regions, identified by VEP but not considered by the clinical hypothesis, was significantly higher in non-seizure-free patients, one can argue that despite possible false positive detections, some of these regions can be epileptogenic, notably in cases with surgery failure. This situation is illustrated in the clinical Use Case 3, where a nonresected region detected by VEP was also identified as epileptogenic by whole brain functional imaging approaches (MEG, high-resolution EEG), suggesting including this VEP region in a resection plan of a second surgery. Alternatively, these regions could represent important hubs of the propagation network, highly interconnected with the EZN. This hypothesis is in good agreement with a recent study on structural connectome hubs in temporal lobe epilepsy showing that patients with abnormally integrated structural network nodes were less likely to achieve seizure freedom.⁵⁰ Hence, these somehow surprising results, when corroborated by other imaging modalities, are not only of additional diagnostic value but of particular importance as potential targets for network-aiming treatment strategies, for example, SEEG-guided thermocoagulations or transcranial direct current stimulation.⁵¹

The major advantage of the VEP approach compared to other recently proposed model-based methods, such as neural fragility,²⁵ is that VEP works on the whole brain source spaces instead of the sensor recording spaces alone. Beyond the brain model's role as a target for data fitting in VEP, the personalized brain model bears promise to serve as a digital twin, in which clinical hypotheses and treatment options are tested in computer simulations. This potential remains to be exploited in neuroscience, medicine, and neurotechnology.

4.1 | Limitations of the actual VEP model

Below, we discuss most pertinent limitations revealed by the analysis of VEP performances at an individual patient level, and eventual solutions to be considered for future VEP developments.

First, there are technical limitations inherent to the use of an automated brain parcellation. Although the VEP atlas has demonstrated good precision, comparable with other available atlases,³³ parcellation errors were observed in the presence of brain surface distortions due to a postoperative or posttraumatic resection cavity, or an extended lesion that impacts gyration pattern (e.g., ischemic lesion, polymicrogyria, schizencephaly). Another technical limitation is that the hypothalamus and the heterotopic gray matter, where epileptogenic lesions such as hypothalamic hamartoma and periventricular nodular heterotopia can be located, are not included in the actual parcellation scheme of the VEP atlas. These limitations should be considered for future development of the VEP atlas. Second, there are some limitations due to the low resolution of the current NMM approach, which reduces source activity to a single node mapped to one of 162 VEP regions. Any grouping cancels the directionality of the current dipole of the folded cortical sheet, which may result in wrong mapping from sources to sensors and thus possibly introduce errors into the estimation of the EZN. In particular, in several cases, we noticed an equal contribution of sources from some deep cortical regions and the neighboring subcortical nuclei (e.g., the posterior insula and the putamen, the orbitofrontal cortex and the caudate nucleus) to the same sensor within the respective cortical region. The solution is to use high-resolution virtual brain models,⁵² where each node corresponds to one vertex of 260 000 and provides a spatial resolution of 1 mm.² The high resolution provides a more realistic source to sensor mapping by considering the detailed cortical/subcortical geometry and both the orientation and the distance between the dipoles and the sensor.

In conclusion, quantification of the epileptogenic networks is a crucial diagnostic step that is valuable in research and in clinical practice. VEP uses personalized virtual brain model methods by integrating epilepsy patient-specific anatomical data with functional data to aid in clinical decision-making by estimating the EZN. An actual VEP model shows good precision in detecting epileptogenic regions; limitations at the individual level should be worked out. The ongoing multicenter trial is essential to understand these limitations and to estimate the impact of VEP on improving surgical prognosis. Future directions are VEP modeling based on noninvasive data fitting, *in silico* surgery, and exploration of personalized brain stimulation approaches.

AUTHOR CONTRIBUTIONS

Fabrice Bartolomei and Viktor Jirsa: Conceptualization and design of the study. Julia Makhalova, Fabrice Bartolomei, Samuel Medina Villalon, Huifang Wang, and Maxime Guye: Data acquisition. Julia Makhalova,

Samuel Medina Villalon, Huifang Wang, Bernard Giusiano, Christian Bénar, and Fabrice Bartolomei: Data analysis. Huifang Wang and Marmaduke Woodman: VEP workflow pipeline and software. Samuel Medina Villalon: Software. Julia Makhalova, Samuel Medina Villalon, Fabrice Bartolomei: Original draft and figures. Julia Makhalova, Huifang Wang, Samuel Medina Villalon, Maxime Guye, Christian Bénar, Viktor Jirsa, and Fabrice Bartolomei: Review and editing of the manuscript.

ACKNOWLEDGMENTS

This work is funded through the European Union's Horizon 2020 Framework Program for Research and Innovation under the Specific Grant Agreement No. 945539 (Human Brain Project SGA3) and the French National Research Agency as part of the second Investissements d'Avenir program (ANR-17-RHUS-0004, EPINOV). We thank Dr Cristina Filipescu for her help with data collection; Dr Elodie Garnier for her help with statistical analysis; Pr Didier Scavarda and Dr Romain Carron for the surgical management of included patients; and Pr Agnès Trebuchon, Dr Aileen McGonigal, and Dr Nathalie Villeneuve for the clinical management of some included patients.

CONFLICT OF INTEREST

None of the authors has any conflict of interest to disclose. We confirm that we have read the Journal's position on issues involved in ethical publication and affirm that this report is consistent with those guidelines.

ORCID

Julia Makhalova  <https://orcid.org/0000-0001-7962-2942>

Fabrice Bartolomei  <https://orcid.org/0000-0002-1678-0297>

REFERENCES

- Jehi L, Friedman D, Carlson C, Cascino G, Dewar S, Elger C, et al. The evolution of epilepsy surgery between 1991 and 2011 in nine major epilepsy centers across the United States, Germany, and Australia. *Epilepsia*. 2015;56(10):1526–33. <https://doi.org/10.1111/epi.13116>
- Baud MO, Perneger T, Rácz A, Pensel MC, Elger C, Rydenhag B, et al. European trends in epilepsy surgery. *Neurology*. 2018;91(2):e96–e106. <https://doi.org/10.1212/WNL.00000000000005776>
- Alomar S, Jones J, Maldonado A, Gonzalez-Martinez J. The stereo-electroencephalography methodology. *Neurosurg Clin N Am*. 2016;27(1):83–95. <https://doi.org/10.1016/j.nec.2015.08.003>
- Jayakar P, Gotman J, Harvey AS, Palmini A, Tassi L, Schomer D, et al. Diagnostic utility of invasive EEG for epilepsy surgery: indications, modalities, and techniques. *Epilepsia*. 2016;57(11):1735–47. <https://doi.org/10.1111/epi.13515>
- Jehi L, Morita-Sherman M, Love TE, Bartolomei F, Bingaman W, Braun K, et al. Comparative effectiveness of stereotactic electroencephalography versus subdural grids in epilepsy surgery. *Ann Neurol*. 2021;90(6):927–39. <https://doi.org/10.1002/ana.26238>
- Isnard J, Taussig D, Bartolomei F, Bourdillon P, Catenoux H, Chassoux F, et al. French guidelines on stereoelectroencephalography (SEEG). *Neurophysiol Clin*. 2018;48(1):5–13. <https://doi.org/10.1016/j.neucli.2017.11.005>
- Cardinale F, Rizzi M, Vignati E, Cossu M, Castana L, d'Orio P, et al. Stereoelectroencephalography: retrospective analysis of 742 procedures in a single centre. *Brain*. 2019;142(9):2688–704. <https://doi.org/10.1093/brain/awz196>
- Lagarde S, Buzori S, Trebuchon A, Carron R, Scavarda D, Milh M, et al. The repertoire of seizure onset patterns in human focal epilepsies: determinants and prognostic values. *Epilepsia*. 2019;60(1):85–95. <https://doi.org/10.1111/epi.14604>
- Bartolomei F, Nica A, Valenti-Hirsch MP, Adam C, Denuelle M. Interpretation of SEEG recordings. *Neurophysiol Clin*. 2018;48(1):53–7. <https://doi.org/10.1016/j.neucli.2017.11.010>
- Perucca P, Dubeau F, Gotman J. Intracranial electroencephalographic seizure-onset patterns: effect of underlying pathology. *Brain*. 2014;137(1):183–96. <https://doi.org/10.1093/brain/awt299>
- Pizzo F, Roehri N, Catenoux H, Medina S, McGonigal A, Giusiano B, et al. Epileptogenic networks in nodular heterotopia: a stereoelectroencephalography study. *Epilepsia*. 2017;58(12):2112–23. <https://doi.org/10.1111/epi.13919>
- Bartolomei F, Lagarde S, Wendling F, McGonigal A, Jirsa V, Guye M, et al. Defining epileptogenic networks: contribution of SEEG and signal analysis. *Epilepsia*. 2017;58(7):1131–47. <https://doi.org/10.1111/epi.13791>
- Bartolomei F, Chauvel P, Wendling F. Epileptogenicity of brain structures in human temporal lobe epilepsy: a quantified study from intracerebral EEG. *Brain*. 2008;131(Pt 7):1818–30. <https://doi.org/10.1093/brain/awn111>
- David O, Blauwblomme T, Job AS, Chabardès S, Hoffmann D, Minotti L, et al. Imaging the seizure onset zone with stereoelectroencephalography. *Brain*. 2011;134(Pt 10):2898–1. <https://doi.org/10.1093/BRAIN/AWR238>
- Gnatkovsky V, De Curtis M, Pastori C, Cardinale F, Lo Russo G, Mai R, et al. Biomarkers of epileptogenic zone defined by quantified stereo-EEG analysis. *Epilepsia*. 2014;55(2):296–305. <https://doi.org/10.1111/EPI.12507>
- Grinenko O, Li J, Mosher JC, Wang IZ, Bulacio JC, Gonzalez-Martinez J, et al. A fingerprint of the epileptogenic zone in human epilepsies. *Brain*. 2018;141(1):117–31. <https://doi.org/10.1093/BRAIN/AWX306>
- Talairach J, Bancaud J. Lesion, “irritative” zone and epileptogenic focus. *Confin Neurol*. 1966;27(1):91–4. <https://doi.org/10.1159/000103937>
- Bancaud J, Angelergues R, Bernouilli C, Bonis A, Bordas-Ferrer M, Bresson M, et al. Functional stereotaxic exploration (SEEG) of epilepsy. *Electroencephalogr Clin Neurophysiol*. 1970;28:85–6.
- Rosenow F, Lüders H. Presurgical evaluation of epilepsy. *Brain*. 2001;124(Pt 9):1683–700. <https://doi.org/10.1093/BRAIN/124.9.1683>
- Lüders HO, Najm I, Nair D, Widdess-Walsh P, Bingman W. The epileptogenic zone: general principles. *Epileptic Disord*.

- 2006;8(Suppl 2):S1–9. <https://doi.org/10.3109/9780203091708-107>
21. Spencer SS. Neural networks in human epilepsy: evidence of and implications for treatment. *Epilepsia*. 2002;43(3):219–27. <https://doi.org/10.1046/J.1528-1157.2002.26901.X>
 22. Spencer DD, Gerrard JL, Zaveri HP. The roles of surgery and technology in understanding focal epilepsy and its comorbidities. *Lancet Neurol*. 2018;17(4):373–82. [https://doi.org/10.1016/S1474-4422\(18\)30031-0](https://doi.org/10.1016/S1474-4422(18)30031-0)
 23. Goodfellow M, Rummel C, Abela E, Richardson MP, Schindler K, Terry JR. Estimation of brain network ictogenicity predicts outcome from epilepsy surgery. *Sci Rep*. 2016;6:29215. <https://doi.org/10.1038/srep29215>
 24. Jirsa VK, Proix T, Perdikis D, Woodman MM, Wang H, Gonzalez-Martinez J, et al. The virtual epileptic patient: individualized whole-brain models of epilepsy spread. *Neuroimage*. 2017;145:377–88. <https://doi.org/10.1016/j.neuroimage.2016.04.049>
 25. Li A, Huynh C, Fitzgerald Z, Cajigas I, Brusko D, Jagid J, et al. Neural fragility as an EEG marker of the seizure onset zone. *Nat Neurosci*. 2021;24(10):1465–74. <https://doi.org/10.1038/s41593-021-00901-w>
 26. Sinha N, Dauwels J, Kaiser M, Cash SS, Brandon Westover M, Wang Y, et al. Predicting neurosurgical outcomes in focal epilepsy patients using computational modelling. *Brain*. 2017;140(2):319–32. <https://doi.org/10.1093/brain/aww299>
 27. Wendling F, Benquet P, Bartolomei F, Jirsa V. Computational models of epileptiform activity. *J Neurosci Methods*. 2016;260:233–51. <https://doi.org/10.1016/j.jneumeth.2015.03.027>
 28. Sanz-Leon P, Knock SA, Spiegler A, Jirsa VK. Mathematical framework for large-scale brain network modeling in the virtual brain. *Neuroimage*. 2015;111:385–430. <https://doi.org/10.1016/j.neuroimage.2015.01.002>
 29. Proix T, Bartolomei F, Guye M, Jirsa VK. Individual brain structure and modelling predict seizure propagation. *Brain*. 2017;140:641–54. <https://doi.org/10.1093/brain/awx004>
 30. Hashemi M, Vattikonda AN, Sip V, Guye M, Bartolomei F, Woodman MM, et al. The Bayesian virtual epileptic patient: a probabilistic framework designed to infer the spatial map of epileptogenicity in a personalized large-scale brain model of epilepsy spread. *Neuroimage*. 2020;217:116839. <https://doi.org/10.1016/j.neuroimage.2020.116839>
 31. Vattikonda AN, Hashemi M, Sip V, Woodman MM, Bartolomei F, Jirsa VK. Identifying spatio-temporal seizure propagation patterns in epilepsy using Bayesian inference. *Commun Biol*. 2021;4(1):1244. <https://doi.org/10.1038/s42003-021-02751-5>
 32. Colombet B, Woodman M, Badier JM, Bénar CG. AnyWave: a cross-platform and modular software for visualizing and processing electrophysiological signals. *J Neurosci Methods*. 2015;242:118–26. <https://doi.org/10.1016/j.jneumeth.2015.01.017>
 33. Wang HE, Scholly J, Triebkorn P, Sip V, Medina Villalon S, Woodman MM, et al. VEP atlas: an anatomic and functional human brain atlas dedicated to epilepsy patients. *J Neurosci Methods*. 2021;348:108983. [doi:10.1016/j.jneumeth.2020.108983](https://doi.org/10.1016/j.jneumeth.2020.108983)
 34. Tournier JD, Smith R, Raffelt D, Tabbara R, Dhollander T, Pietsch M, et al. MRtrix3: a fast, flexible and open software framework for medical image processing and visualisation. *Neuroimage*. 2019;202:116137. [doi:10.1016/J.NEUROIMAGE.2019.116137](https://doi.org/10.1016/J.NEUROIMAGE.2019.116137)
 35. Jirsa VK, Stacey WC, Quilichini PP, Ivanov AI, Bernard C. On the nature of seizure dynamics. *Brain*. 2014;137:2210–30. <https://doi.org/10.1093/brain/awu133>
 36. Sarvas J. Basic mathematical and electromagnetic concepts of the biomagnetic inverse problem. *Phys Med Biol*. 1987;32(1):11–22. <https://doi.org/10.1088/0031-9155/32/1/004>
 37. Medina Villalon S, Paz R, Roehri N, Lagarde S, Pizzo F, Colombet B, et al. EpiTools, a software suite for presurgical brain mapping in epilepsy: intracerebral EEG. *J Neurosci Methods*. 2018;303:7–15. <https://doi.org/10.1016/j.jneumeth.2018.03.018>
 38. Lagarde S, Roehri N, Lambert I, Trebuchon A, McGonigal A, Carron R, et al. Interictal stereotactic-EEG functional connectivity in refractory focal epilepsies. *Brain*. 2018;141(10):2966–80. <https://doi.org/10.1093/brain/awy214>
 39. Barba C, Barbati G, Minotti L, Hoffmann D, Kahane P. Ictal clinical and scalp-EEG findings differentiating temporal lobe epilepsies from temporal “plus” epilepsies. *Brain*. 2007;130(7):1957–67. <https://doi.org/10.1093/brain/awm108>
 40. Wendling F, Bartolomei F, Bellanger JJ, Bourien J, Chauvel P. Epileptic fast intracerebral EEG activity: evidence for spatial decorrelation at seizure onset. *Brain*. 2003;126(Pt 6):1449–59. <https://doi.org/10.1093/brain/awg144>
 41. Andrzejak RG, David O, Gnatkovsky V, Wendling F, Bartolomei F, Francione S, et al. Localization of epileptogenic zone on pre-surgical intracranial EEG recordings: toward a validation of quantitative signal analysis approaches. *Brain Topogr*. 2014;28(6):832–7. <https://doi.org/10.1007/S10548-014-0380-8>
 42. Balatskaya A, Roehri N, Lagarde S, Pizzo F, Medina S, Wendling F, et al. The “Connectivity Epileptogenicity Index” (CEI), a method for mapping the different seizure onset patterns in StereoElectroEncephalography recorded seizures. *Clin Neurophysiol*. 2020;131(8):1947–55. <https://doi.org/10.1016/j.clinph.2020.05.029>
 43. Nissen IA, Stam CJ, van Straaten ECW, Wotschel V, Reijneveld JC, Baayen JC, et al. Localization of the epileptogenic zone using interictal MEG and machine learning in a large cohort of drug-resistant epilepsy patients. *Front Neurol*. 2018;9:647. <https://doi.org/10.3389/fneur.2018.00647>
 44. Varotto G, Susi G, Tassi L, Gozzo F, Franceschetti S, Panzica F. Comparison of resampling techniques for imbalanced datasets in machine learning: application to epileptogenic zone localization from interictal intracranial EEG recordings in patients with focal epilepsy. *Front Neuroinform*. 2021;15:715421. <https://doi.org/10.3389/fninf.2021.715421>
 45. Nissen IA, Millán AP, Stam CJ, van Straaten ECW, Douw L, Pouwels PJW, et al. Optimization of epilepsy surgery through virtual resections on individual structural brain networks. *Sci Rep*. 2021;11(1):19025. <https://doi.org/10.1038/s41598-021-98046-0>
 46. Kini LG, Bernabei JM, Mikhail F, Hadar P, Shah P, Khambhati AN, et al. Virtual resection predicts surgical outcome for drug-resistant epilepsy. *Brain*. 2019;142(12):3892–905. <https://doi.org/10.1093/brain/awz303>
 47. An S, Bartolomei F, Guye M, Jirsa V. Optimization of surgical intervention outside the epileptogenic zone in the virtual epileptic patient (VEP). *PLoS Comput Biol*. 2019;15(6):e1007051. <https://doi.org/10.1371/JOURNAL.PCBI.1007051>
 48. Olmi S, Petkoski S, Guye M, Bartolomei F, Jirsa V. Controlling seizure propagation in large-scale brain networks. *PLoS*

- Comput Biol. 2019;15(2):e1006805. <https://doi.org/10.1371/JOURNAL.PCBI.1006805>
49. Job AS, David O, Minotti L, Bartolomei F, Chabardès S, Kahane P. Epileptogenicity maps of intracerebral fast activities (60–100 Hz) at seizure onset in epilepsy surgery candidates. *Front Neurol.* 2019;10:1263. <https://doi.org/10.3389/FNEUR.2019.01263>
50. Gleichgerrcht E, Keller SS, Drane DL, Munsell BC, Davis KA, Kaestner E, et al. Temporal lobe epilepsy surgical outcomes can be inferred based on structural connectome hubs: a machine learning study. *Ann Neurol.* 2020;88(5):970–83. <https://doi.org/10.1002/ANA.25888>
51. Yang D, Wang Q, Xu C, Fang F, Fan J, Li L, et al. Transcranial direct current stimulation reduces seizure frequency in patients with refractory focal epilepsy: a randomized, double-blind, sham-controlled, and three-arm parallel multicenter study. *Brain Stimul.* 2020;13(1):109–16. <https://doi.org/10.1016/j.brs.2019.09.006>
52. Jirsa VK. Neural field dynamics with local and global connectivity and time delay. *Philos Trans R Soc A Math Phys Eng Sci.* 1891;2009(367):1131–43. <https://doi.org/10.1098/rsta.2008.0260>

SUPPORTING INFORMATION

Additional supporting information may be found in the online version of the article at the publisher's website.

How to cite this article: Makhalova J, Medina Villalon S, Wang H, Giusiano B, Woodman M, Bénar C, Virtual epileptic patient brain modeling: Relationships with seizure onset and surgical outcome. *Epilepsia.* 2022;63:1942–1955. <https://doi.org/10.1111/epi.17310>